




Article

Multi-Analytical Characterization of Corvins' Castle—Deserted Tower. Construction Materials and Conservation Tests

Rodica Mariana Ion ^{1,2,*}, Lorena Iancu ^{1,2}, Madalina Elena David ^{1,2},
Ramona Marina Grigorescu ¹, Bogdan Trica ¹, Raluca Somoghi ¹, Sorina Florentina Vasile ¹,
Ioana Daniela Dulama ³, Anca Irina Gheboianu ³ and Sorin Tincu ⁴

¹ Research Group “Evaluation and Conservation of Cultural Heritage”, National R&D Institute for Chemistry and Petrochemistry—ICECHIM, 202 Splaiul Independentei, 060021 Bucharest, Romania; lorena.iancu@icechim.ro (L.I.); madalina.david@icechim.ro (M.E.D.); ramona.grigorescu@icechim.ro (R.M.G.); bogdan.trica@icechim.ro (B.T.); raluca.somoghi@icechim.ro (R.S.); sorina.vasile14@icechim.ro (S.F.V.)

² Materials Engineering Department, Doctoral School of Materials Engineering, Valahia University of Târgoviște, 130105 Târgoviște, Romania

³ Institute of Multidisciplinary Research for Science and Technology, Valahia University of Târgoviște, 13 Sinaia Alley, 130004 Târgoviște, Romania; dulama.ioana@icstm.ro (I.D.D.); anca@icstm.ro (A.I.G.)

⁴ Corvins' Castle, 331141 Hunedoara, Romania; sorin_tincu@yahoo.com

* Correspondence: rodica.ion@valahia.ro; Tel.: +40-21-316-3094

Received: 9 July 2020; Accepted: 19 August 2020; Published: 20 August 2020



Abstract: The aim of this paper is to analyze the construction materials (mortars) of an architectural monument (Deserted Tower (Lilly Tower) from Corvins' Castle, Romania). The mortars were characterized following a multidisciplinary approach, combining macroscopic observation with petrographic microscopy, mineralogical analysis (X-ray diffraction) and elemental analysis (X-ray fluorescence), hydric properties, and color of representative samples of the monument. The results revealed the use of gypsum mortars (produced by lumps with higher Fe content), with minor concentrations of crystalline dolomites of the Southern Carpathians, calcite, and quartz. The materials' effective porosity and their water absorption capacity were high. A possible solution to consolidate the damaged area with some consolidation products (hydroxyapatite carbonate and its derivatives with Ag and Sr) was investigated, too. The interactions between the mortar's specimens and the effectiveness of the consolidation treatments were evaluated by physico-chemical analyses (molecular structure by X-ray powder diffraction (XRPD), wavelength dispersive X-ray fluorescence (WDXRF), dynamic light scattering (DLS)), morphological characterization by microscopic techniques as SEM-EDS, TEM, and physical and mechanical investigations (peeling test and compressive strength). Results were drawn based on historical, in situ observations, and analytical data, and put into evidence the composition, high weathering degree, and the possibility to surface consolidate with Sr-CHAP.

Keywords: mortar; Corvins' Castle—Deserted Tower; conservation; restoration

1. Introduction and Historical Settings

From ancient times, stones have been used as material for different monuments and artworks, mainly due to their proper characteristics (composition, texture, resistance, porosity, aesthetic aspects, etc.). For conservation and restoration, some operations are required in order to identify the original composition, structure, and to recover the aesthetic aspect of different monuments [1]. Under this context, the characterization of the construction materials is essential for all specialists

involved in the monument's maintenance. However, the construction stone cohesion is affected by different degradation processes, such as cracking or mineral component disintegration under the influence of some decay agents such as humidity, thermal shock, and salt crystallization, many of them being provoked by environmental conditions (temperature, humidity, and salt presence) or human interventions.

The materials science allows the optimization of materials to adapt them to their current use and environmental conditions. Petrological and petrophysical properties, like effective porosity, bulk density, water absorption capacity, and ultrasonic pulse velocity, determine construction materials' quality, durability, and decay [1,2].

Even if the used techniques were not identical for all types of stone (with similar composition), they showed complementarities and offer important conclusions on the archaeometric characterization of the stones and useful recommendations of consolidant materials for the monument surface treatment. Furthermore, some techniques require a big amount of the sample from the monument, which is practically impossible to obtain without destroying the original monument.

The Corvins' Castle, also known as the Hunyadi Castle, is a Gothic-Renaissance castle in Hunedoara. It was given to John Hunyadi's father in 1409 by Sigismund, King of Hungary, and its reconstruction began in 1446 when John Hunyadi was elected regent governor of the Kingdom of Hungary [3]. Based on a fourteenth-century stone fortress, John Hunyadi transformed the military building into a gothic style building. After John Hunyadi died in 1456, the castle work stopped until 1458, when numerous Renaissance elements were added in the building architecture. In 1480, work was completely stopped, and even so, the castle was recognized as being one of the biggest and most impressive buildings in Eastern Europe [4,5].

The overall appearance is due to the restoration works from the XIXth century to the XXth century, some of them without any compatibility reasons between the used materials. Now, the castle is a large and imposing structure with tall towers, bastions, an inner courtyard, diversely colored roofs, and myriads of windows and balconies adorned with stone carvings, as shown in Figure 1.



(a)

Figure 1. Cont.



(b)

Figure 1. Photos of Corvins' Castle (a) and Deserted Tower (DT) (b): up from left to right: DT interior face of the castle; middle and right: DT exterior face of the castle; down: the main weathering forms.

The restoration works executed between the end of the XIXth and early XXth centuries may have caused more harm than good, as original elements of the Western palace were destroyed and “faithfully” reconstructed by Ferenc Schulcz, while other elements were “restored” more creatively. By 1874, the architect Imre Steindl had reimagined the monument and added roof tiles, archways, and the Ioan de Hunedoara statue atop the Painted Tower, raised the roof level with various vaulted ceilings, and contributed a variety of features (e.g., crenellations, a small tower) reminiscent of the castle’s origins as a fortification. After 1874, architects plastered the insides and outsides of the buildings and recycled sculptural material as masonry [6]. Finally, in 1907, Istvan Möller restored the western and northern wings of the castle as accurately as possible, relying on archaeological excavations, drawings from L. Arányi, and rescuing repurposed fragments of sculpture from previous reconstructions. Möller’s work was interrupted by the outbreak of World War I, when he was no longer able to continue the work on the castle [7]. After Romania gained the territory of Transylvania through the Treaty of Trianon in 1920, the president of the Transylvania branch of the Romanian Historical Monuments Commission, Alexandru Lepadatu, decided to cease all restoration works in Corvins’ Castle [8].

From 1956 to 1968, the Diet Hall (*Sala Dietei*), Knight’s Hall (*Sala Cavalerilor*), and chapel have been successfully restored to commemorate the 500 year anniversary of Ioan de Hunedoara’s death in 1956 [6,9]. After this period, no restoration campaigns focused on more than one wing or room of the castle. Archaeological excavations inside the castle (including the courtyard and sacristy) confirm the historical record of occupation from the XVth to XVIIth centuries, though excavations outside the walls of the castle find the archaeological record disturbed by the restoration works and construction debris of the XIXth and XXth centuries [10].

The Deserted Tower (known as Lilly Tower) is one of the most damaged towers from this monument (eight towers), and its investigation is absolutely necessary—the last restoration being in the XXth century.

The circular towers (Capistrano Tower, Deserted Tower, Tobosarilor Tower) were provided with a solid masonry ground floor, followed by two levels of defense (with a diameter of 6 m); the bottom ones being used as rooms for riflemen and the upper ones, as living areas and/or defense areas.

From the structural point of view, the assembly presents a conglomerate of buildings with different volumes and height regimes, but without corresponding structural links between them. The fortification walls are made in six different historical stages, between the XIVth and XVIIIth centuries and with architectural styles characteristic of that period of time. The basic material used for the fortress and later

for the Corvins' Castle was the dolomitic limestone. In the first stage of the execution of the fortress in the XIVth century, stone blocks from the river were positioned directly on the rock. The choice of dolomitic limestone as a building stone has been admitted by two main reasons—the existence of limestone quarries nearby and utilizing of these rocks in fortification buildings [11].

The crude stone used for this castle should have been as clean as possible, strong, compact, and adhering well to the mortar. From the XVIth century, brick has been used for this building and after 1960 cement has been used for some restoration procedures at this tower [12].

The previous papers reported the presence of the plaster, dolomite of small size, large blocks of dolomitic limestone, summary shaped, bound with mortar, porous mortar with residues of dolomite, and ground black soil containing prehistoric material where the foundations have been dug [13]. Given the historical importance of this monument and the lack of archaeometric studies and details needed to continue the restoration procedures, a complex archaeometric investigation is required to be made to report the materials used in these towers, their degradation, and techniques to build this monument [14,15].

During the last decades, multiple interdisciplinary studies with analytical techniques have been published in the cultural heritage field [16–18]. New and modern techniques have been adopted for the study of objects, including non-invasive methodologies like wavelength dispersive X-ray fluorescence (WDXRF), which allows the determination of the major and minor elements and a selected number of trace elements of the investigated sample [19], X-ray powder diffraction (XRPD), as the most popular technique for determining mineral phases [20], and in some cases, the products of degradation processes, generated by the environmental pollution [21].

Besides all these techniques, microscopy techniques are used too, as follows—optical microscopy (OM), scanning electron microscopy (SEM)—in order to investigate the internal morphology and topology, and the pore structure [22].

An efficient consolidant product should obey the specific characteristics of the artwork (chemical composition, physical properties, state of deterioration, etc.) and its preserving conditions (temperature, relative humidity, etc.), for maintaining the aesthetic value, in agreement with the Venice Charter (1964) [23–25].

Homogeneous distribution of the consolidant, with minimal contrasting interfaces, minimize the stone's tendency to crack and dry [26] with harmful effects. Although the consolidation action could be found to significant depths (2 to 3 cm) [27], the consolidation action, however, remains very low for some preserved monuments. However, for improving the consolidation, following the decision of the archaeologists to use traditional materials, a new trend to use new and compatible materials and nanomaterials, especially, is observed today.

The term *compatibility* was introduced at the Dahlem conference [28]. For a consolidant to be compatible, it means that treatments or introduced materials will not have negative consequences from the technical, aesthetical, or historical point of view. Reasoned replacement of natural stone in historic buildings has been common practice in conservation campaigns over the years [29]. The use of cement consequences used as restoration materials during the last two restoration campaigns carried out during the XXth century at Corvins' Castle—Deserted Tower are analyzed in this paper and adequately discussed.

The effects of the new consolidants have been evaluated through the adequate investigation techniques: X-ray powder diffraction (XRPD), wavelength dispersive X-ray fluorescence (WDXRF), scanning electron microscopy with electronic dispersive spectroscopy (SEM-EDS), optical microscopy (OM), transmission electron microscopy (TEM), dynamic light scattering (DLS) for size and Z-potential, Brunauer–Emmett–Teller (BET) for molecular structure, composition, morphology, and also mechanical properties (compressive strength and roughness). The chromatic parameters, water repellence, penetration of water, wettability, and salt crystallization effect on the durability of investigated stone materials, have been investigated, too.

2. Materials and Methods

2.1. Construction Materials

A visual inspection was made on the mortars collected from the Deserted Tower (DT). Two types of mortars have been identified, as follows:

M1 is the masonry mortar, mixed colored: light grey, light brown, and white, as shown in Figure 2. Its aggregates, observable with the naked eye, are homogeneous and without preferential orientation.



Figure 2. Samples from Corvins' Castle—DT: (M1 and M2) masonry mortars. M1 is collected from the inside of the tower, while M2 is collected from outside of the castle.

M2 is the masonry mortar with a light grey binder. Its aggregates are slightly lighter than the matrix, homogeneously distributed, and without preferential orientation.

Except these, a whitish with light color tones (light yellow/whitish) coating mortar has been identified, distributed homogeneously, without preferential orientation, in some places covering the original surfaces (probably from the previous restoration procedure), as shown in Figure 2.

2.2. Sampling and Macroscopic Characterization

After sampling the DT stones, the main forms of degradation were identified, visible through surface deposits (accumulation of dust, soil, black crusts, patinas (black and orange), and surface recession with detached crusts and differential erosion (mainly in the lower part of the tower), gaps and crevices). For ethical reasons, a very small number of samples of small size and without heritage value were taken, which do not affect the integrity of the monument. A map of weathering types is shown in Figure 1b.

2.3. Testing Methods

The peeling test has been applied in order to evaluate the cohesion on the surface samples, after the Drdácý et al. method [30], with additional steps mentioned in Scrivano et al. [31], using Scotch Crystal tape (3M) with 10 repetitions over the same location. After approximately 90 s of application

with constant pressure (2 kgf/cm²), the tape was removed by taking hold of the free end and pulling it off steadily (not jerkily) at a rate of about 10 mm/s and at an angle of 90°. After weighing, the samples were analyzed by microscopy (using a STEREOBLUE stereomicroscope) and ImageJ software was used to mark and calculate the detached area from each sample. The percentage of consolidation (% C) was calculated according to Equation (1) [32]:

$$\% C = (TRM_{untreated} - TRM_{treated}) / TRM_{untreated} * 100 \quad (1)$$

where $TRM_{untreated}$ is the total amount of material removed by peeling in the untreated sample, g and $TRM_{treated}$ is the total amount of material removed in the treated sample, g.

Carbonation testing was performed using phenolphthalein solution (1 g phenolphthalein + 70 mL ethanol + 30 mL water), observing the color change to bright pink.

For mechanical tests, the Schmidt hammer as a portable device has been used for evaluating the mechanical resistance of stone. The rebound number can be converted to uniaxial compressive strength (UCS) that, according to Wang and Yuan [33], can be correlated to a qualitative evaluation of stone hardness. UCS (MPa) can be calculated using Equation (2):

$$UCS = 10^{0.0088 \cdot \bar{N} \cdot \gamma + 1.01} \quad (2)$$

where \bar{N} is the average of the rebound correction value (ΔN_a) for the measuring angle of 90° ($\Delta N_a = -0.0012 \cdot N^2 + 0.1725 \cdot N - 8.975$), and γ is the stone density, g/cm³, determined by the immersion method according to EN 1015-10 [34] and has a value of 1.504 g/m³.

For the water absorption test, the samples were dried in the oven at 40 °C for 8 h, cooled at room temperature, and then weighed (W_1). After that, the samples were immersed in distilled water for 24 h. In the end, they were removed from distilled water and weighed (W_2). The water absorption content was calculated with Equation (3).

$$WA = \frac{W_2 - W_1}{W_1} * 100 \quad (3)$$

2.4. Consolidant Derivatives and Application Method

The carbonated hydroxyapatite (CHAp) and its metallic derivatives (Me-CHAp) (Ag-CHAp and Sr-CHAp) consolidants, used in this work, were obtained as described in our previous work [15]. CHAp was synthesized from $(NH_4)_2HPO_4$, NH_4HCO_3 , and $Ca(NO_3)_2 \cdot 4H_2O$, under magnetic stirring, adjusting the pH to 11, at room temperature. After filtering the generated precipitate, the reaction product was freeze-dried overnight and calcinated at 900 °C for 4 h. Ag-CHAp and Sr-CHAp were synthesized by a similar microemulsion method, but using the appropriate metal nitrate solutions ($AgNO_3$, $Sr(NO_3)_2$), at a concentration of 5 mol. % related to Ca^{2+} .

Then, 0.25 g/L of CHAp and Me-CHAp were dispersed in water and the solutions were ultrasonicated for 60 min at 40 °C and applied by brushing 3 times on each sample face. The applications were performed under controlled conditions (50% RH, $T = 20$ °C, airspeed <0.1 m/s) on the pre-cleaned samples with a soft brush. Mechanical cleaning is not recommended due to the friability of the mortars.

2.5. Analytical Methods

The wavelength dispersive X-ray fluorescence spectrometry (WDXRF) was performed in order to provide the qualitative and quantitative elementary composition and to complete the chemical analysis of samples. The system is equipped with 3 crystal analyzers (with automated exchange): LiF (200) for heavy elements (Ti-U), PET and RX 25 pt light elements (O-Mg and Al-Sc) with 200 W power (50 kV tens, 4 mA int). Detection limit: 1 ppm–10 ppb; accuracy <0.1–0.5%; the elements were ranging from 8 O to 92 U.

The X-ray powder diffraction (XRPD) have been recorded with an X-ray diffractometer Rigaku Ultima IV, the main parameters being: vertical goniometer θ/θ (285 mm radius) in geometry G/9; X-ray tube—Cu anode (2 kW); detector—NaI; Bragg-Brentano with high-resolution geometry; software: PDXL 2.2. (processing), ICDD-PDF4+2016 (database). The Rietveld method for the whole powder pattern fitting (WPPF) was used to refine crystal structure parameters (atom coordinates, temperature factors, etc.) based on the diffraction pattern.

The petrographic analysis was conducted on an Olympus BH-2 petrographic microscope, using 4× and 10× magnifications.

Dynamic light scattering (DLS) served for measuring the particle size and Z potential through a Zetasizer Nano ZS, Malvern Instruments Ltd., U.K. equipment. Analyses were performed on colloidal dispersion in isopropyl alcohol; field device for measuring the particle size is 0.6 nm–6 μ m; field for zeta potential: 5 nm–10 μ m, at a scattering angle of 90° and 25 °C temperature, using intensity distribution. The Z-potential measurements of the nanoparticles were recorded by applying an electric field across the analyzed aqueous dispersions using the appropriate accessory of the Zetasizer. All measurements were performed in triplicate.

Porosity determinations have been recorded at 77 K in the relative pressure range $p/p_0 = 0.005$ –1.0 using a NOVA2200e Gas Sorption Analyzer (Quantachrome, Boynton Beach, FL, USA) and the data were processed using the NovaWin version 11.03 software. Prior to adsorption measurements, the samples were degassed for 4 h at 180 °C under vacuum. The specific surface area was determined by the standard Brunauer–Emmett–Teller (BET) equation. The total pore volume was estimated from the volume adsorbed at a relative pressure p/p_0 close to unity. Pore size distribution and mesoporous volume were obtained from the desorption branch of the isotherm by applying the Barrett–Joyner–Halenda (BJH) model. The t-plot method was used to estimate the micropore surface area and external surface area. These measurements were performed on irregular samples.

The optical microscopy was performed with a Novex trinocular microscope (EUROMEX Microscope B.V.HOLLAND) (at different magnifications: 40×, 100×, 400×, 1000×). A CFI60 infinity optical system was attached to provide a high quality, compact, and easy-to-use polarizing microscope. The equipment has a digital video camera attached that allows real-time data acquisition. Furthermore, a Stereo microscope StereoBlue (EUROMEX Microscope B.V.HOLLAND), with Zoom stereo 0.7× to 4.5× objective has been used.

The scanning electron microscopy with energy dispersive spectroscopy (SEM-EDS) data were obtained by a SU-70 (Hitachi, Japan) microscope coupled with an UltraDry detector (Thermo Fisher Scientific, United States of America). The image enhancement through colorization, 3D reconstruction, and the evaluation of roughness parameters were performed with dedicated scanning electron microscopy software (ImageJ NIH Software-free demo).

The transmission electron microscopy (TEM) was achieved using a G2 F20 TWIN Cryo-TEM (Philips, Netherlands), with an accelerating voltage of 200 keV, for analyzing the morphology of the particles. After being dried at room temperature, the samples have been dispersed and ultrasonicated in distilled water. A small droplet of the aqueous dispersion was put on a carbon grid, without staining, and microscopically examined.

The chromatic parameters have been recorded with a Konica Minolta CR-410 colorimeter, Japan, for calculation of the total color differences ΔE^* ; ΔL^* is the difference in lightness ($\Delta L^* = L^*_{\text{treated stone}} - L^*_{\text{control}}$), Δa^* is the chromatic deviation of the a coordinates (red and green color) ($\Delta a^* = a^*_{\text{treated stone}} - a^*_{\text{control}}$), and Δb^* is chromatic deviation of the b coordinates (yellow and blue color) ($\Delta b^* = b^*_{\text{treated stone}} - b^*_{\text{control}}$) [35].

3. Results

3.1. In Situ Measurements and Observations

The Corvins' Castle is located in the area of Paleozoic crystalline dolomites of the Southern Carpathians, and so other metamorphic rocks, such as mica schists, quartzites, gneisses, and graphitic schists, can be found on the geological map [36,37]. The sample of stone (A) is a whitish colored sample, with sand-size grains with a colored coating from iron oxides, knowing that this area is iron-rich, and recognized as a metallurgical area. The mortar samples from inside are light grey, without preferential orientation, with real damaged areas, gaps, and crevices (A, B), while the outside mortar is white, with traces of bricks glued to them and with exterior surface black, most probably due to environmental damages (C, D). From the mineralogical point of view, the composition of DT includes dolomite, quartz, calcite, and micas, similar to the literature results [38,39]. A small slice of the sample as evidence of the composition of the tower is shown in Figure 3.

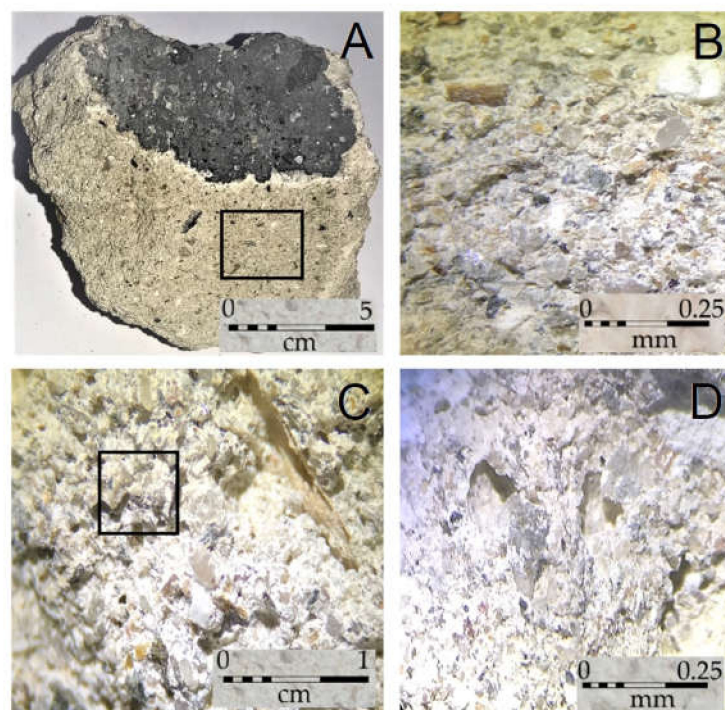


Figure 3. Main mortar types used (A, B: M2; C, D: M1).

In the case of petrographic components, a distinction was made between the aggregates from the bonding phase, determining their mineralogy and identifying ceramic, coal, and vegetable fragments. The petrographic determinations examined the porosity and size and shape characteristics. These tests help to understand the behaviors of stone materials in contact with water, their capacity to absorb water, or to cause its evaporation, knowing that the alteration processes depend on water circulation inside porous solids, and based on them ascertaining the age and durability of mortars.

M1 has aggregates composed mostly of quartz with the size around 100–200 μm , with vegetal fragments. M2 has aggregates from quartz fragments and pores without any filling, as shown in Figure 4. This last sample has been detached from a brick most probably used at the last restoration work.

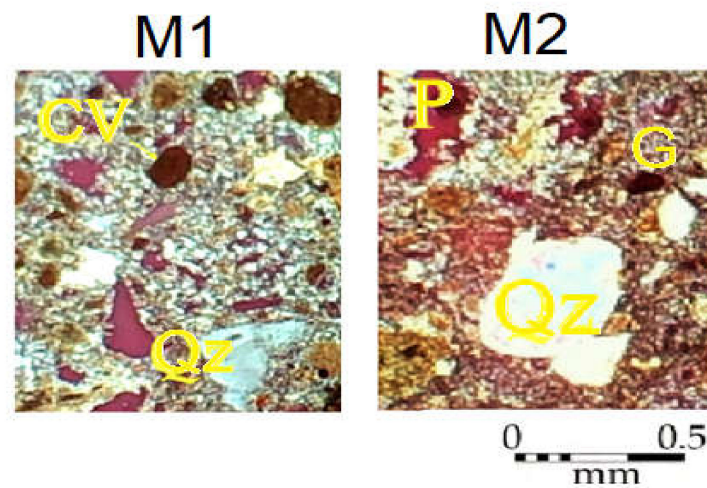


Figure 4. The microscopy image of the sample collected from DT (Qz = quartz; P = pore; L = lump; CV = calcined vegetable; G = Gypsum): mortars (M1, M2). The lumps could be identified as impurities from bricks possibly used at the recent restoration works.

The presence of calcite, quartz, dolomite, gypsum etc. in different proportions could be proved by EDS technique, too, with the results presented in Figure 5 and Table 1. The mineralogical analysis with XRPD indicated the presence of these minerals, as shown in Figure 6 and Table 2.

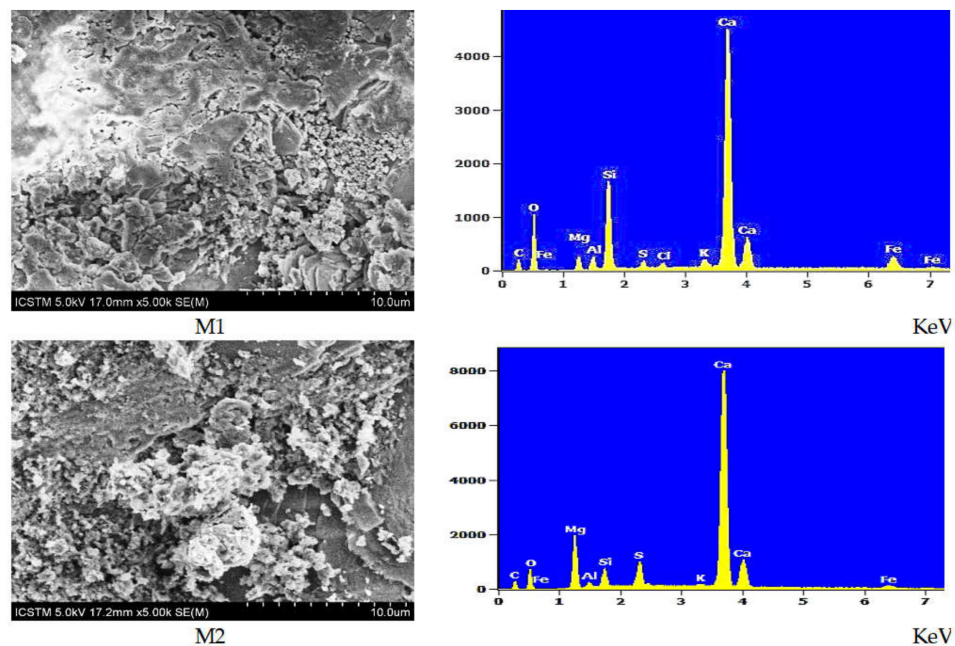
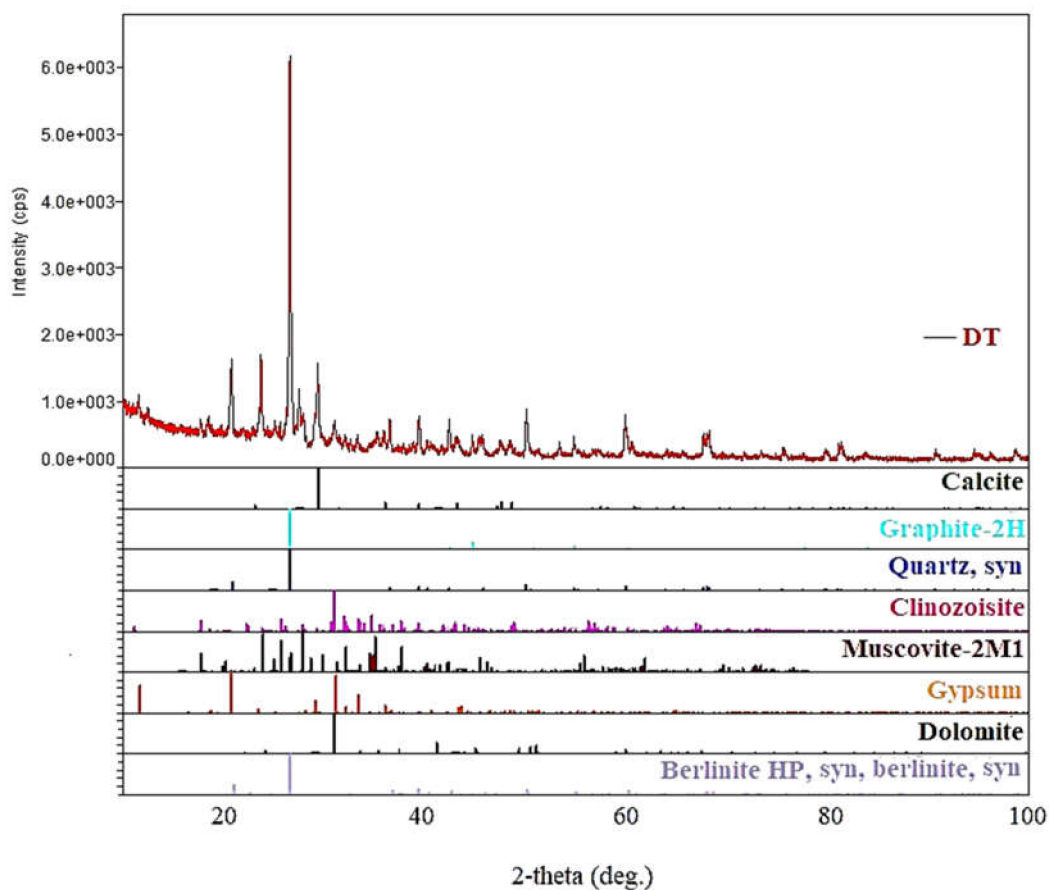


Figure 5. FE-SEM images of the DT samples recorded at Vacc = 5 kV, WD = 18.4–18.7 mm, 3000× magnification (M1 and M2). The EDS patterns of the DT samples—the main element compositions are labeled (M1 and M2).

Table 1. The elemental composition of Corvins' Castle—Deserted Tower.

Sample	Composition (wt % \pm Error %) ¹									
	C	O	Mg	Al	Si	S	Cl	K	Ca	Fe
M1	5.68 \pm 0.2	35.70 \pm 0.54	1.57 \pm 0.06	1.32 \pm 0.04	8.42 \pm 0.09	0.69 \pm 0.03	0.48 \pm 0.05	0.98 \pm 0.04	38.64 \pm 0.27	6.51 \pm 0.31
M2	5.95 \pm 0.16	25.74 \pm 0.46	8.58 \pm 0.08	0.81 \pm 0.04	0.81 \pm 0.04	3.56 \pm 0.05	n.d. ²	0.27 \pm 0.04	50.40 \pm 0.28	2.23 \pm 0.22

¹ The detection and quantification were done with K-lines (for all elements) and the composition was normalized to 100 wt %; ² n.d.—element which was not detected in sample.

**Figure 6.** The X-ray powder diffraction (XRPD) diagram for the mortar sample with a Rietveld processing diagram.**Table 2.** XRPD peaks information.

No.	2-Theta (deg.)	d (ang.)	Phase Name
1.	17.772	4.987	Muscovite-2M1 (0,0,4)
2.	20.842	4.259	Quartz, syn (1,0,0), Clinozoisite (0,0,2), Muscovite-2M1 (1,1,1), Berlinite HP, syn, berlinite, syn (1,0,0)
3.	23.732	3.746	Muscovite-2M1 (0,2,3)
4.	26.607	3.347	Quartz, syn (1,0,1), Clinozoisite (0,1,2), Muscovite-2M1 (0,2,4)
5.	25.502	3.241	Graphite-2H (0,0,2), Clinozoisite (1,0,2), Berlinite HP, syn, berlinite, syn (0,0,3)

Table 2. Cont.

No.	2-Theta (deg.)	d (ang.)	Phase Name
6.	29.970	2.979	Clinozoisite (3,0,−2), Muscovite-2M1 (0,2,5)
7.	31.068	2.876	Gypsum (1,1,−2), Calcite (0,0,6), Muscovite-2M1 (1,1,5),
8.	33.300	2.688	Clinozoisite (1,0,−3), Muscovite-2M1 (0,2,6)
9.	35.300	2.541	Gypsum (1,3,−2), Dolomite (0,1,5), Muscovite-2M1 (2,0,0)
10.	36.530	2.458	Quartz, syn (1,1,0), Clinozoisite (2,0,2), Muscovite-2M1 (1,3,−3)
11.	39.402	2.285	Calcite (1,1,3), Quartz, syn (1,0,2), Gypsum (1,5,1), Clinozoisite (0,2,2)
12.	42.407	2.130	Quartz, syn (2,0,0), Muscovite-2M1 (2,2,2)
13.	43.110	2.097	Calcite (2,0,2), Clinozoisite (0,0,4), Muscovite-2M1 (2,2,−4), Berlinite HP, syn, berlinite, syn (1,0,4)
14.	45.762	1.981	Quartz, syn (2,0,1)
15.	47.530	1.911	Calcite (0,2,4), Graphite-2H (1,0,1), Gypsum (1,7,−1), Clinozoisite (4,1,0), Muscovite-2M1 (2,2,−6)
16.	48.420	1.878	Calcite (1,1,6), Gypsum (3,1,−1), Clinozoisite (2,0,−5), Muscovite-2M1 (2,2,5)
17.	50.103	1.819	Quartz, syn (1,1,2), Clinozoisite (1,0,−5)
18.	54.826	1.673	Quartz, syn (2,0,2), Muscovite-2M1 (1,3,−2), Gypsum (2,6,−2)
19.	59.936	1.542	Quartz, syn (2,1,1), Clinozoisite (2,2,−5), Muscovite-2M1 (3,1,4), Dolomite (2,1,−2)
20.	67.677	1.383	Quartz, syn (2,1,2), Gypsum (4,0,−2), Muscovite-2M1 (3,1,7), Dolomite (3,0,0)
21.	68.113	1.375	Quartz, syn (2,0,3), Clinozoisite (0,3,4), Muscovite-2M1 (1,5,−9), Dolomite (0,1,11)
22.	81.160	1.184	Quartz, syn (1,1,4), Muscovite-2M1 (4,0,−8)

3.2. Consolidant Applications

3.2.1. Conservation Proposals

The composition of the not-treated and treated samples with different consolidants has been highlighted by WDXRF, as it is visible in Table 3.

Table 3. Composition of Corvins' Castle—Deserted Tower treated with CHAp derivatives.

Component	DT	DT + CHAp	DT + Ag-CHAp	DT + Sr-CHAp
		wt%		
CaO	21.3589 ± 0.044	44.0349 ± 0.0710	51.3650 ± 1.0360	61.0121 ± 1.6570
SiO ₂	38.9495 ± 0.1324	21.2177 ± 0.0380	21.9194 ± 0.0490	16.1732 ± 0.0390
MgO	12.8629 ± 0.2506	7.9097 ± 0.2500	7.4038 ± 0.2480	7.7009 ± 0.1220
SO ₃	7.7038 ± 0.0361	1.7943 ± 0.0098	0.9783 ± 0.0230	1.7084 ± 0.0180
Al ₂ O ₃	6.655 ± 0.0799	5.5471 ± 0.1320	6.3187 ± 0.0720	4.9450 ± 0.0920
Na ₂ O	n.d.	1.7682 ± 0.0790	1.9661 ± 0.0670	n.d.
Fe ₂ O ₃	9.6387 ± 0.02983	2.2969 ± 0.0290	4.3919 ± 0.0430	3.3747 ± 0.0390
K ₂ O	1.4488 ± 0.04470	1.6287 ± 0.0460	2.2576 ± 0.0270	1.9142 ± 0.0320
P ₂ O ₅	0.3077 ± 0.03871	0.1504 ± 0.0360	0.3241 ± 0.0210	0.5373 ± 0.0260
Cl	0.1567 ± 0.0098	0.3983 ± 0.0440	1.1004 ± 0.0040	0.7842 ± 0.0080
ZrO ₂	0.0384 ± 0.0162	0.1669 ± 0.0290	0.0677 ± 0.0030	0.0485 ± 0.0050
Ag ₂ O	n.d.	n.d.	1.1904 ± 1.2340	n.d.
SrO	0.0629 ± 0.0162	n.d.	n.d.	0.0610 ± 0.0050
Other	0.8167 ± 0.0511	3.087 ± 0.0120	0.717 ± 0.0400	1.7406 ± 0.0600

For understanding the interactions between stone and the consolidation compounds, the comparison between the particle sizes, measured by TEM (for consolidant particles), DLS (average hydrodynamic diameters of the particles), polydispersity index (PDI) (measured by Zetasizer), and the size of the pores (by BET techniques) demonstrated that even CHAp and derivatives have approximately 80 nm and 700 nm (800–7000 Å), as shown in Table 4. The hydrodynamic diameter varies between 285 and 307 Å with pore diameters between 4.0 to 4.2 nm, and the PDI value was between 0.246 and 0.830 nm, thus indicating a narrow and favorable particle size distribution, as shown in Table 4.

Table 4. The parameters indicating the particle size of the consolidant.

Sample	PDI (DLS)	Size, nm (DLS)	Z mV (DLS)	Pore Diameter (nm) (BET)	Surface Area (m ² /g) (BET)	Hydrodynamic Diameter Å (DLS)
CHAp	0.830	955.5	−25.6	4.2	5.8	285.7
Ag-CHAp	0.483	147	−10.3; −30.3	4.085	4.02	307.2
Sr-CHAp	0.246	156.2	−17.6	4.014	4.106	287.7

In Figure 7, SEM images for the samples collected from Corvins' Castle—DT treated with CHAp, Ag-CHAp, and Sr-CHAp are presented.

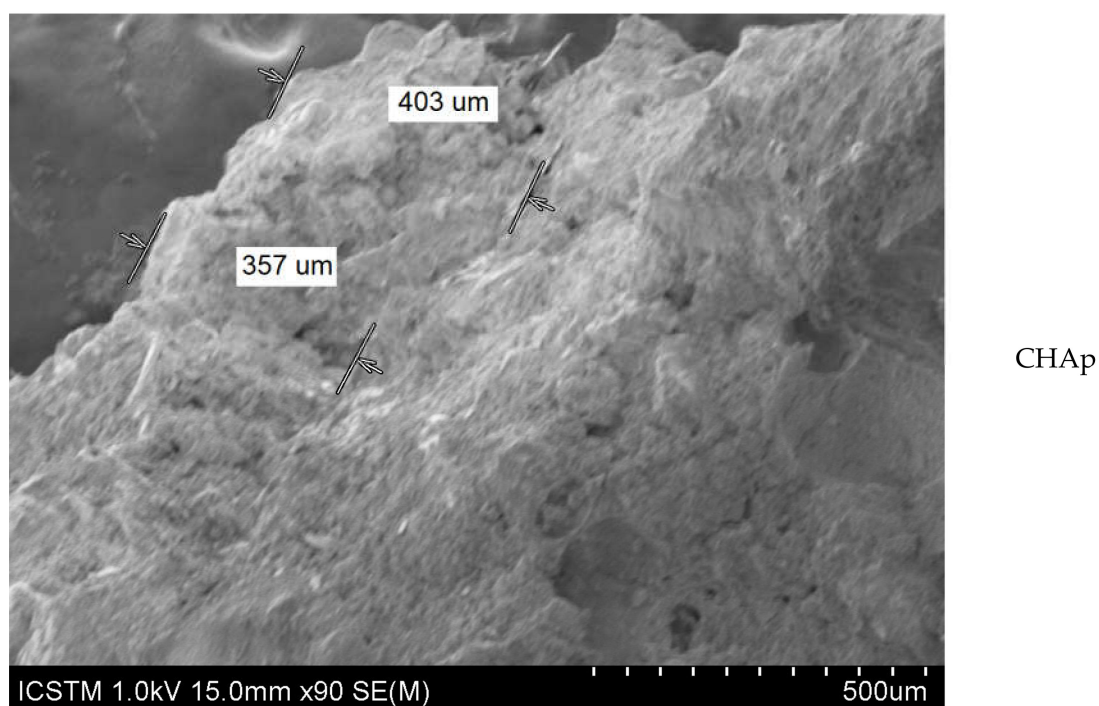


Figure 7. Cont.

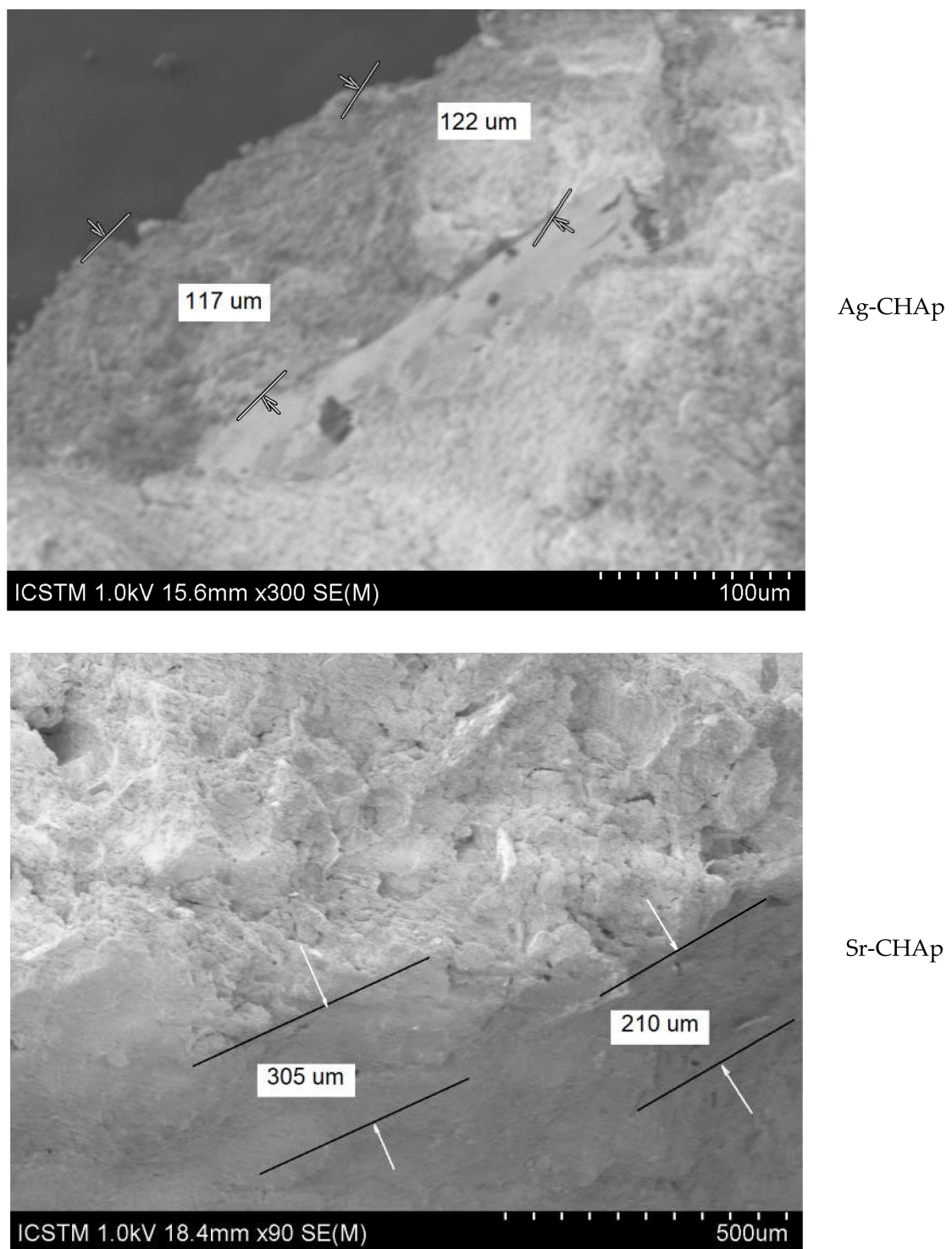


Figure 7. SEM images of mortar treated with CHAp, Ag-CHAp, and Sr-CHAp.

By brushing the carbonated hydroxyapatite derivatives on the samples, some layers with thicknesses between 100 and 400 μm are formed. The thicker layer is visible for Ag-CHAp, most probably due to the agglomeration capacity of this compound. These statements could be proved by the sizes of CHAp derivative particles measured by TEM. The obtained images show semi-spherical shapes, with a polydispersity, and agglomeration of small grains that form a grain of higher dimension, as shown in Figure 8, which is more accentuated for Ag-CHAp than for the others. TEM analysis confirms the presence of the different shape morphology (spherical or irregular polygon) of the prepared CHAp (a) and its derivatives with with Ag (b) or Sr (c). The particles' diameter varies from 100 to 700 nm, as shown in Figure 8.

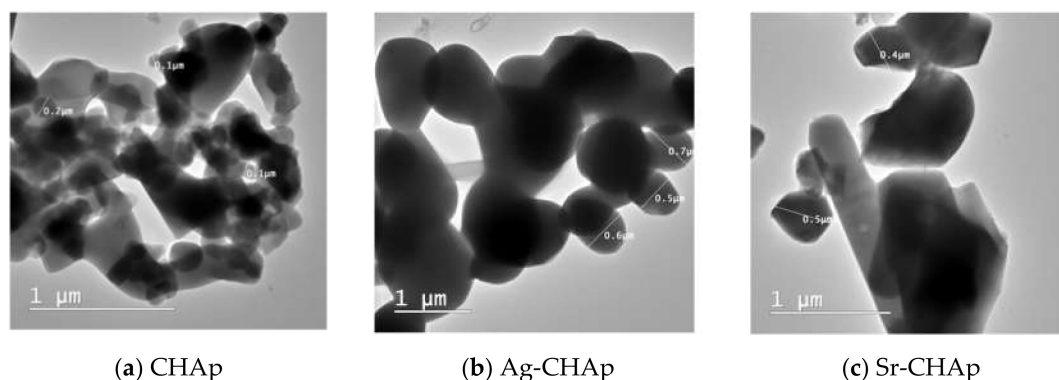


Figure 8. TEM images for CHAp (a), Ag-CHAp (b), and Sr-CHAp (c) particles.

3.2.2. Chromatic Parameters

The aesthetical properties of both the untreated and treated samples have been evaluated by colorimetric examination, on homogenous spots, as shown in Table 5. The values obtained from these measurements demonstrated that the consolidant products, applied by brushing, led to the best results, with $\Delta b^* < 5$, which represent the proper value for a color stable surface [40].

Table 5. Color variation of the treated DT samples (reported to the untreated sample).

Sample	Δb_x	ΔE_x
DT + CHAp	1.95	3.45
DT + Ag-CHAp	1.81	4.05
DT + Sr-CHAp	3.17	4.32

The investigated samples did not show significant color changes; after the treatment with CHAp consolidants, DT samples have a low value for the total color difference (ΔE^*), less than 5. Knowing that the literature indicates a ΔE^* value less than 3 for a good consolidant, and between 3 and 5 for a consolidant with a medium activity [41], it could be concluded that the consolidating product used to treat the DT sample does not significantly affect the stone color parameters after treatment, $\Delta E_x < 5$.

3.2.3. Carbonation Process

In order to check the presence of cement, possibly used at this monument at previous restoration works, the carbonation process has been tested, being one of the most proper processes to put into evidence the main defects in concrete, causing the reinforcement corrosion. Carbon dioxide (CO_2), which is a natural gas present in the air, and sulfur dioxide (SO_2), which is increased by industrial production, can combine with the atmospheric moisture and react with the calcium hydroxide from the concrete producing calcium carbonate and calcium sulphate (gypsum). This chemical process and the material reaction attack the concrete and reduce the natural alkalinity. The pH value of pure water in

the hardened cement paste, of about 13, will be reduced to around 9.0. Phenolphthalein is an acid–base indicator which can be extremely useful for carbonation testing. The solution will turn into bright pink if it interacts with an alkaline compound. As unaffected concrete has a high pH, after the test it will turn pink, but if the concrete is carbonated, it will remain uncolored. It should be noted that the pink color indicates that enough $\text{Ca}(\text{OH})_2$ is present, but it may have been carbonated to a lesser extent. The test is covered by a specific standard [42].

After performing the test with phenolphthalein solution (1 g phenolphthalein + 70 mL ethanol + 30 mL water) it can be observed that the areas exposed to the solution remained colorless, which means that the pH in the respective area is lower than 8.6 (suggesting carbonation), as shown in Figure 9. All these visual observations could be an indicator of the different restoration actions by using cement or concrete-based materials, which previously occurred at this tower.

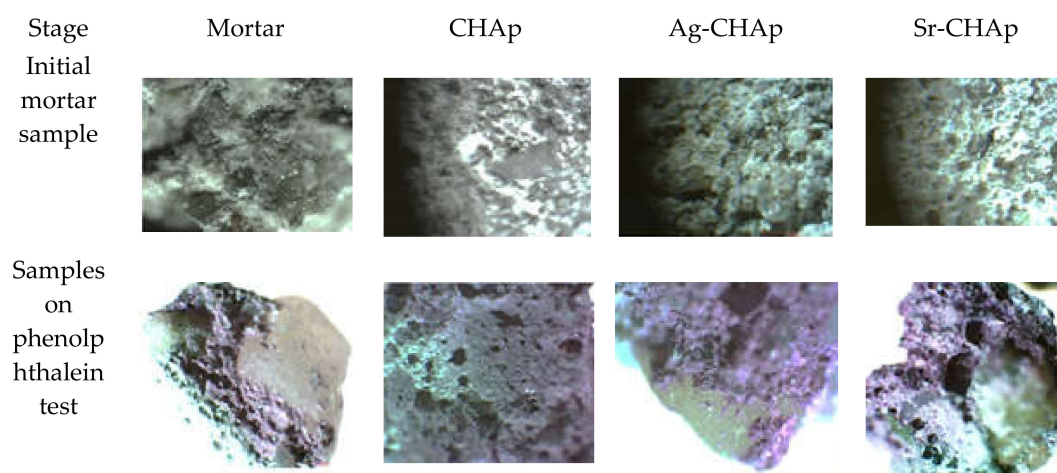


Figure 9. Phenolphthalein tests for non-treated and treated DT samples.

3.2.4. Roughness Parameters

The sample collected from Corvins' Castle—DT has a uniaxial compressive strength of 7.92 MPa, so it is a soft stone (corresponding to a UCS between 15 and 5 MPa). Being a soft stone, no additional mechanical measurement was possible, so only a visual comparison of the estimated surface roughness of the investigated samples was preferred, generated based on the SEM images, using a dedicated image enhancing software. The microstructural surface features of the material are suggestively presented in Figure 10, in which the valleys marked with dark blue indicate the location of the pores within the material and the peaks marked with red are a predictor of the higher roughness of the material. Red peaks were observed mostly for samples treated with Ag-CHAp and Sr-CHAp, indicating a higher roughness of the material. The results presented in Figure 10 offer a general perspective on the surface roughness. It was observed that the historical surface of Sr-CHAp was closer to the control one.

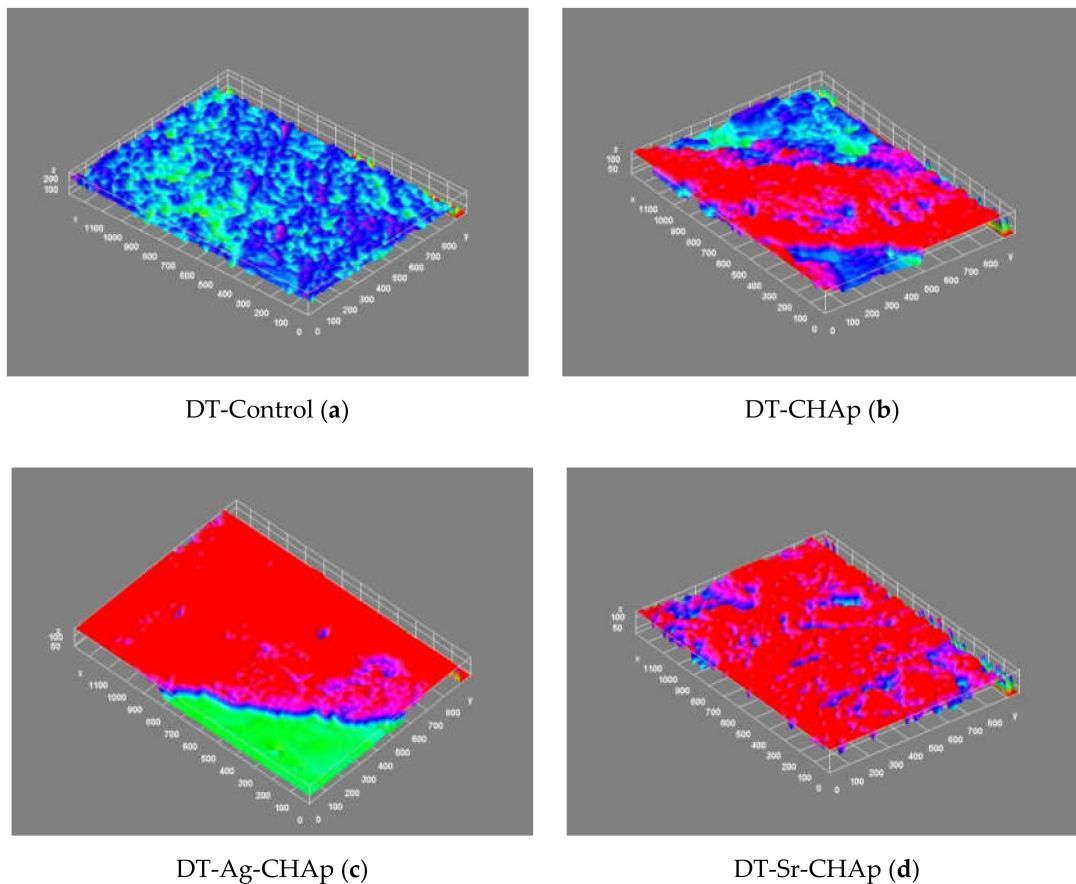


Figure 10. Estimated surface roughness using ImageJ.

For local roughness analysis on the whole surface, the roughness values according to the ISO 4287/2000 standard [43,44] were measured. The values of the most representative roughness parameters (R_q —root mean square deviation and SA —surface area, given in calibrated units) recorded for DT treated samples are presented in Table 6.

Table 6. Roughness parameters and pore surface area for the treated and not-treated samples.

Sample	R_q	SA
Not-treated	45.574	5.6089
CHAp	43.164	4.5657
Ag-CHAp	40.9166	8.9172
Sr-CHAp	41.1277	5.3291

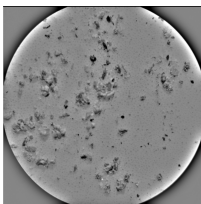

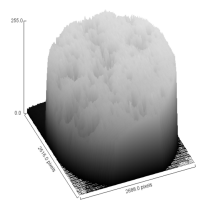
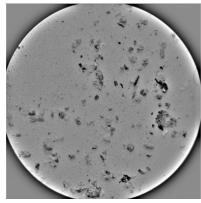
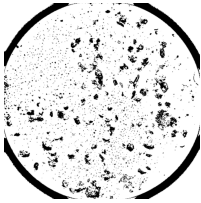
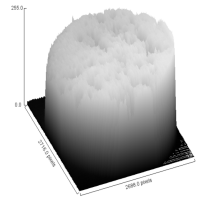
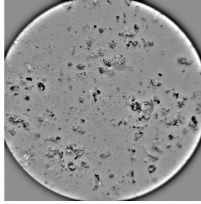
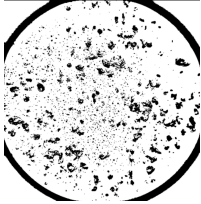
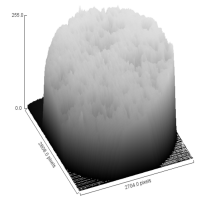
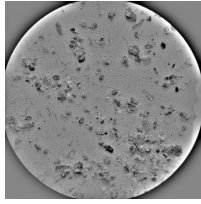

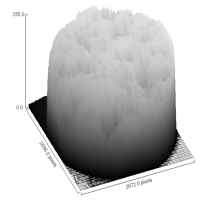
The average surface roughness of the treated specimens is slightly modified. The consolidating product fills the pores and inter-crystalline grain contacts. The analyses reveal that the roughness parameters could be in good correlation with surface area and physical and hydric properties of the stones, as shown in Table 7.

Table 7. Water absorption capacity for the treated and control DT samples.

Sample	Absorption, %
DT	13.4304
DT + CHAp	16.0617
DT + Ag-CHAp	13.7955
DT + Sr-CHAp	12.5797

In Table 8, the consolidation action of CHAp and its metallic derivatives on the DT sample by microscopic image, the contouring and the calculating result of the detached area (DA) from the tested surfaces, the depth of surface plotter, and the percent of consolidation (PC) ensured by treatment can be analyzed.

Table 8. Peeling consolidation test for DT samples.

Sample	MO (2X Magnification)	Image Reconstruction	Image 3D Reconstruction	DA, %	PC, %
Control				8.61	-
CHAp				5.54	52.85
Sr-CHAp				5.81	48.57
Ag-CHAp				5.15	53.42

4. Discussion

On-site measurements and observations showed that the DT was poorly maintained and partially damaged. Even if the mortars are quite similar in terms of texture and composition, there are many differences between the various portions of the tower, most likely due to local interventions over time. The petrographic analyses of the mortars show some differences in size and shape—lumps, and carbonated and siliceous aggregates, which may suggest that the quartz areas may come either from the crushing of carbonated stones or from the crushing of more siliceous stones.

The measurements and observations carried out in situ have shown a damaged and poorly maintained area for this tower. A slow connection between stone and brick, connected with mortar is

observed. The detached surface of these samples is related to the presence of mortar residues, which keep the traces of the dismantled bricks, which are slightly alveolar.

In this context, diffractograms of untreated mortars showed mostly the presence of gypsum, dolomite, calcite, muscovite, clinozoisite, and graphite etc. X-ray fluorescence showed that this mortar has a high Fe content, possibly of the present in this area, which is known as a metallurgical area. The energy-dispersive spectroscopy (EDS) analyses of the elemental composition of the studied samples, as shown in Figure 5, revealed some proportion of Ca, O, and C and a minor proportion of Si, K, Mg, and Al (in all studied samples). The high content of Ca that was detected in the samples can be explained by a higher quantity of calcite phases in those samples. Some amounts of sulfates have been detected on the exterior face of the tower, as a result of the weather factors damaging the surface in time.

Weathering is often divided into different forms of weathering—physical weathering (known as mechanical weathering or disaggregation), due to temperature, pressure, frost etc., causing the disintegration by abrasion, cracks, erosion, etc., chemical weathering (oxidation, solubilization, and hydrolysis processes), due to water and oxygen, and biological weathering, involving the weakening and subsequent breakdown by plants, animals, and microbes of rock, generating holes and gaps that develop as this process continues, exposing the stone to physical and chemical weathering.

These data indicated the susceptibility to degradation of construction materials due to high water absorption. After studying the water behavior of construction materials, the amount of water taken can depend mainly on the amount and shape of the pores. The material with the highest porosity was the material with the highest water absorption, and the material with the lowest porosity was the material with the lowest water absorption.

The high values of water absorption capacity presented in Table 6 support this possibility. In addition, the crystallization of salts and the freeze–thaw behavior over time have led to a loss of cohesion and granular disintegration of its building materials and a weakening of the structure.

Since inorganic consolidants used in the form of spray are necessary for the consolidation of the mortar surfaces, based on the expertise of our group, we performed in situ tests for the treatment of DT mortars with carbonated hydroxyapatite and its strontium and silver derivatives.

For potential applications in the preservation and restoration of cultural heritage objects, hydroxyapatite (HAp) has been used as a good consolidant agent for various types of artefacts: stone, paper, and wood [14,45–48]. The selection of HAp as a potential material for the protection and consolidation of carbonate stones was based on its low solubility and slow dissolution rate [15,49]. The carbonated hydroxyapatite is more adequate for surface consolidation, especially for carbonated limestone, by comparison with all the other inorganic consolidants. By comparison with HAp, which has a crystal structure very similar to that of calcite, enabling epitaxial growth over calcareous matrices, in carbonated hydroxyapatite (CHAp) the CO_3^{2-} ions can replace both OH^- and PO_4^{3-} ions and thus the last form has a higher special surface area than the previous one [50].

Compared to alternative products from the market, the treatment with carbonated hydroxyapatite offers some advantages:

Ammonium oxalate has low penetration (1–2 mm) [51]; ammonium ions may alter pigments (verdigris, malachite, etc.); it has a much lower solubility than calcite or gypsum, yet permeable to water (liquid-vapor), and is remarkably resistant in acidic environments.

Ethyl silicate shows a mechanical strengthening for a long period, keeps the treated stone hydrophobic for several months, and induces some alterations in the pore system and is of chromatic aspect; often applied in organic solvents (e.g., white spirit), which can be toxic for human health and the environment [52].

Phosphates present low viscosity, are able to penetrate deeply into weathered marble (>20 mm) and limestone (>25 mm), and can lead to significant mechanical strengthening after curing for a short time (24–48 h). Moreover, no significant altered porosity and pore size distribution, or any changes in water absorption, drying rate, and water vapor permeability were observed; better durability at freeze–thaw cycles, and at salt crystallization cycles was obtained; also, no significant color change and any toxic released compounds were recorded [53].

By comparison with the compounds above-mentioned, the CHAp powder, previously prepared by our group, showed better homogeneity and a better consolidating effect, in spite of its higher solubility (0.0092 g/L) by comparison with HAp (0.0003 g/L) [49]. The mechanical properties of CHAp have been greatly improved by doping CHAp with different metal ions [47,54].

The hydrodynamic diameter is typically larger than the diameter measured by TEM, because, in addition to the core of the particle, it takes into account also the surface structure and ions. Furthermore, the surface area (BET) (m^2/g) is between 9.211 for DT (mortar) to 5.8 (CHAp), 4.02 (Ag-CHAp), and 4.106 (Sr-CHAp). DT has the pore diameter of 4.053 nm, including waters of hydration. In our experience, the mortar has pores approximately 50% larger than the physical diameter. This could indicate that these aggregates are the stable ones and the larger aggregates are formed through their collisions [55]. The zeta potential of CHAp derivative-loaded stone can greatly influence their stability in suspension by means of electrostatic repulsion between the particles. Our results demonstrated that the zeta potentials of CHAp and CHAp derivative-loaded stone are of -10 and -30 mV, as proof of moderate stability in water. Excepting this, it should be taken into account that Ag-CHAp is able to associate and generate large particles, and this could be demonstrated by two Z values, corresponding to the presence of two bands.

In our previous paper, it was reported that the synthesis and complex characterization of carbonated hydroxyapatite derivatives (CHAp) and its metallic derivatives (Ag, Sr, Ba, K, Zn), characterized through several analytical tools; also, their coating capacity on some stone samples prepared in the laboratory have been tested, confirming the presence of AB-carbonated type CHAp [15].

Taking into account that CHAp (Me-CHAp; Me = Ag, Sr) samples proved the best effectiveness on stone samples prepared in the laboratory, we intend to continue our investigations by studying the influence of these consolidants on the stone samples from historical Corvins' Castle, Hunedoara, Romania (Deserted Tower), in order to find an optimum consolidation treatment for restoration of historical stones.

These properties were reported as the most important roughness parameters for various carbonated hydroxyapatite materials. R_a , which is the arithmetical mean roughness value (the arithmetical mean of the absolute values of the profile deviations from the mean line of the roughness profile) varied between 0.1 and 0.2 μm , with higher values for the samples treated with carbonated hydroxyapatite. While the values of the reported parameters did not differ significantly, the highest values were obtained for the samples treated with Sr-CHAp. These results quantify the findings presented through the 3D reconstruction of the sintered topography and can be used to roughly predict the behavior of the materials—although the phenomena are incompletely understood, higher surface roughness values for hydroxyapatite were reported to influence in a positive way the peeling test, as shown in Table 8. As can be seen in Table 8, the percentage of the detached material was influenced by the consolidant type, and the sample treated with Sr-CHAp presents the lower amount of detached material coupled with the highest percent consolidation compared to DT. Moreover, these results are sustained by the image reconstruction of the detached material obtained after the peeling test.

The lowest C values show the highest consolidation capacity. In our case, even the highest value of C is for Sr-CHAp, while the samples treated with Ag-CHAp have a C (%) of 48.57%; this parameter takes into account the aggregation of Ag-CHAp and states the improvement in cohesion achieved by each treatment (put into evidence by TEM measurements).

For this purpose, several samples produced in the laboratory were microscopically characterized, consolidated, and artificially weathered by salt crystallization tests. To evaluate their consolidating effectiveness, a systematic approach, the peeling test or the so-called “scotch tape test” (STT) was used.

The wettability and hydrophilicity of the samples collected from the Deserted Tower proved a good surface wetting, with the smallest value being for Sr-CHAp, too. This last compound seems to be the best consolidant for such a purpose.

By a carbonation process, it was possible to put into evidence the main defects in concrete, which cause the mortar damages. For this reason, phenolphthalein was used as an acid–base indicator for carbonation testing. As unaffected concrete has a high pH, after the test it will turn pink, but if the concrete is carbonated, it will remain uncolored [42]. The fact that only some parts of the mortars remained uncolored means that in time some reparations occurred with the possible application of cement. The pink color is a sign of the carbonation process, due to the cement presence.

Being a soft stone, no additional mechanical measurement was possible, so it was preferred that only a visual comparison of the estimated surface roughness of the investigated samples was conducted, generated based on the SEM images, using dedicated image enhancing software. The microstructural surface features of the material are suggestively presented in Figure 10, in which the valleys marked with dark blue indicate the location of the pores within the material and the peaks marked with red are a predictor of the higher roughness of the material (Sr-CHAp was closer to the control one).

The average surface roughness of the treated specimens is slightly modified. The consolidating product fills the pores and inter-crystalline grain contacts, and the analyses reveal that the roughness parameters could be a good correlation with surface area and physical and hydric properties of the stones.

These data indicated that the weathering (physical, chemical, and biological) occurred at this tower, as follows: The deposition of exogenous pollutants and their crystallization at the surface lead to the filling of the micropores, and the newly formed crusts can have a higher density than the damaged host mortar. Meanwhile, some black crusts and patinas that could be formed by the deposition of pollutants in the air and carbon particles resulting from the exhaust emissions of vehicles and heavy metals have been recorded. They can fill the smallest surface pores. Nevertheless, a higher value of BET area presumes a higher chemical reactivity, identified by larger areas accessible to decomposition processes. However, it may lead to a decrease in microporosity by preventing further absorption of water vapor and dissolved pollutants. It is better for concrete to have smaller pores, which favors lower moisture content of the condensate.

5. Conclusions

The influence of carbonated hydroxyapatite and its derivatives with Ag and Sr on historical samples collected from Corvins’ Castle, Hunedoara, Romania (Deserted Tower) have been evaluated in this paper.

TEM analysis confirms the diameter of the particles of carbonated hydroxyapatite derivatives from 100 to 400 nm. Particle sizes, measured by TEM (for consolidant particles), by DLS (average hydrodynamic diameters of the particles), PDI (measured by Zetasizer), and the size of the pores (by BET techniques) demonstrated that even CHAp and derivatives have sizes of approximately 80 and 700 nm (8–70 Å); the hydrodynamic diameter varies between 285 and 307 Å with pore diameters between 4.0 to 4.2 Å; the PDI value was between 0.246 and 0.830 nm, thus indicating a narrow size and a favorable particle size distribution. The hydrodynamic diameter is typically larger (approximately 5% larger than the physical diameter) than the diameter measured by TEM, because it takes into account the surface structure and ions.

The zeta potentials of CHAp derivatives and CHAp derivative-loaded stone are of -10 and -30 mV, as proof of moderate stability in water. Excepting this, it should be taken into account that Ag-CHAp is able to associate and generate large particles, and this could be demonstrated by two Z values, corresponding to the presence of two bands.

By treating the real stones with carbonated hydroxyapatite consolidants, no significant change in color was obtained. The estimated surface roughness of the investigated samples was generated based on the SEM images using dedicated image enhancing software. It was observed mostly for samples treated with Ag-CHAp and Sr-CHAp, with a higher roughness of the material.

The best percentage of consolidation (% C) was achieved for the Corvins' Castle dolomitic calcareous treated by Sr-CHAp (51.42%), while on the samples treated with Ag-CHAp, it was 48.57%. This parameter takes into account the aggregation of Ag-CHAp and states the improvement in cohesion achieved by each treatment.

The wettability and hydrophilicity of the samples collected from the Deserted Tower proved a good surface wetting, with the smallest value being for Sr-CHAp, too. This last compound seems to be the best consolidant for such a purpose.

The sample collected from the Deserted Tower from Corvins' Castle has a UCS of 7.92 MPa, so it is a soft rock (corresponding to a uniaxial compressive strength between 15 and 5 MPa).

After performing the test with phenolphthalein solution, it can be observed that the areas exposed to the solution remained colorless, which means that the pH in the respective area is lower than 8.6 (suggesting carbonation), due to the cement or concrete-based materials used for previous restoration or consolidation of this tower.

Under these conditions, the carbonated hydroxyapatite derivatives (Ag, Sr) exhibit the best consolidation effectiveness for the samples collected from the Deserted Tower from Corvins' Castle.

Author Contributions: Conceptualization, R.M.I.; S.T.; and L.I.; methodology, R.M.I.; software, M.E.D.; validation, R.M.I., S.T.; L.I.; and R.M.G.; formal analysis, M.E.D.; investigation, I.D.D.; A.I.G.; B.T.; R.S.; and S.F.V.; resources, R.M.I.; data curation, M.E.D.; writing—original draft preparation, R.M.I.; writing—review and editing, M.E.D.; L.I.; and R.M.I.; visualization, R.M.I.; supervision, R.M.I.; project administration, R.M.I.; funding acquisition, R.M.I. All authors have read and agreed to the published version of the manuscript.

Funding: This research was funded by Romanian Ministry of Research and Innovation, CCCDI—UEFISCDI, grant number 51PCCDI/2018.

Acknowledgments: This work was supported by a grant of the Romanian Ministry of Research and Innovation, CCCDI—UEFISCDI, project number PN-III-P1-1.2-PCCDI-2017-0476/51PCCDI/2018, within PNCI III.

Conflicts of Interest: The authors declare no conflict of interest.

References

1. Van den Eynde, V.C.; Mateos, F.J.; Paradelo, R. Degradability of building stone: Influence of the porous network on the rate of dissolution of carbonate and evaporitic rocks. *J. Cult. Herit.* **2013**, *14*, 89–96. [[CrossRef](#)]
2. Gräf, V.; Jamek, M.; Rohatsch, A.; Tschegg, E. Effects of thermal-heating cycle treatment on thermal expansion behavior of different building stones. *Int. J. Rock Mech. Min. Sci.* **2013**, *64*, 228–235. [[CrossRef](#)]
3. Bodochi, I. Castelul Corvinilor în secolul al XVII-lea (1). *Corviniana* **2008**, *XII*, 207–232.
4. Velescu, O. *Castelul de la Hunedoara*; Editura Meridiane: Monumentele Patriei Noastre: Bucuresti, Romania, 1961.
5. Lupescu, R. Domeniul cetății Hunedoara în timpul Hunedorenilor. *MedTrans* **2001–2002**, *VVI*, 7–34.
6. Roman, C.C.; Diaconescu, D.; Tiplic, M. Archaeological excavations at Hunedoara—The Corvins' Castle—The sacristy of the chapel. In *Studii de Istorie Veche si Arheologie: Bibliotheca Archaeologica et Historica Corvinensis—IV*; Matos, C., Ed.; Editura Mereamia Napocae: Hunedoara, Romania, 2004.
7. Bogdan, C. Contribuții arheologice la cunoașterea evoluției Castelului Corvineștilor de la Hunedoara. *BMI* **1970**, *39*, 18–25.
8. Vatasianu, V. Castelul Corvinilor din Hunedoara. *Boabe de Grau* **1933**, *6*, 420–431.
9. Roman, C.C.; Tincu, S. Observations regarding the ecclesiastical complex from Hunedoara—The Corvin's Castle. *Sargetia Acata Musei Devensis Deva, Romania* **2012**, *3*, 243–258.

10. Schilling, R. Historical conclusions about the archaeological excavations at the medieval castle of Hunedoara. *Bul. Monum. Istor.* **1970**, *2*, 55.
11. Ion, R.-M.; Iancu, L.; Grigorescu, R.M.; Tincu, S.; Vasilievici, G.; Ion, N.; Bucurică, I.A.; Teodorescu, S.; Dulama, I.D.; Știrbescu, R.M.; et al. Arhaeometric investigations on ceramic materials from Hunedoara-the court area. *J. Sci. Arts* **2018**, *18*, 471–480.
12. Ion, R.; Iancu, L.; Grigorescu, R.M.; Carutiu, D.T.; Tincu, S.; Ion, N.; Bucurică, I.A.; Teodorescu, S.; Dulama, I.D.; Știrbescu, R.M.; et al. Arhaeometric Concepts and Methods of Intervention on Historical Monument Buildings. *The Case of the Corvins' Castle. IOP Conf. Ser. Mater. Sci. Eng.* **2018**, *374*, 012073.
13. Ion, R.-M.; Tincu, S.; Iancu, L.; Grigorescu, R.M. Investigations of the new gate tower from Corvins' Castle. *IOP Conf. Ser. Mater. Sci. Eng.* **2019**, *572*, 012088. [[CrossRef](#)]
14. Baglioni, P.; Giorgi, R. Soft and hard nanomaterials for restoration and conservation of cultural heritage. *Soft Matter*. **2006**, *2*, 293–303. [[CrossRef](#)] [[PubMed](#)]
15. Ion, R.-M.; Iancu, L.; Vasilievici, G.; Grigore, M.E.; Andrei, R.E.; Radu, G.I.; Grigorescu, R.M.; Teodorescu, S.; Bucurica, I.A.; Ion, M.L.; et al. Ion-Substituted Carbonated Hydroxyapatite Coatings for Model Stone Samples. *Coatings* **2019**, *9*, 231. [[CrossRef](#)]
16. Sabbioni, C. Mechanisms of air pollution damage to stone. In *The Effects of Air Pollution on the Built Environment, Air Pollution Reviews*; Brimblecombe, P., Ed.; Imperial College Press: London, UK, 2003; pp. 63–106.
17. Frahm, E.; Doonan, R.C.P. The technological versus methodological revolution of portable XRF in archaeology. *J. Archaeol. Sci.* **2013**, *40*, 1425–1434. [[CrossRef](#)]
18. Shackley, M.S. An Introduction to X-ray Fluorescence (XRF) Analysis in Archaeology. In *X-ray Fluorescence Spectrometry (XRF) in Geoarchaeology*; Shackley, M., Ed.; Springer: New York, NY, USA, 2011.
19. Cechak, L.T.; Gerndt, J.; Kopecka, I.; Musilek, L. X-ray fluorescence in research on Czech cultural monuments. *Nucl. Instrum. Methods Phys. Res. B* **2004**, *213*, 735–740.
20. Acun, S.; Ariolu, N. A Method for the Preservation and Restoration of the Stones Used in Historical Buildings. *Archit. Sci. Rev.* **2006**, *49*, 143–148. [[CrossRef](#)]
21. Stuart, B.H. *Analytical Techniques in Materials Conservation*; John Wiley & Sons, Ltd.: Hoboken, NJ, USA, 2007; ISBN 0-470-01280-3.
22. Mazzetto, S.; Petruccioli, A. Methods and Techniques Used in Significant Restoration Projects in Qatar. *Stud. Conserv.* **2018**, *63*, 303–314. [[CrossRef](#)]
23. ICOMOS. International Chapter for the Conservation and Restoration of Monuments and Sites (The Venice Chapter 1964). In *Proceedings of the IInd International Congress of Architects and Technicians of Historic Monuments, Venice, Italy, 25–31 May 1964*.
24. Sandis, C. (Ed.) *Cultural Heritage Ethics: Between Theory and Practice*; Open Book Publishers: Cambridge, UK, 2014; ISBN 978-1-78374-067-3.
25. Ricca, M.; Le Pera, E.; Licchelli, M.; Macchia, A.; Malagodi, M.; Randazzo, L.; Rovella, N.; Ruffolo, S.A.; Weththimuni, M.L.; La Russa, M.F. The CRATI Project: New Insights on the Consolidation of Salt Weathered Stone and the Case Study of San Domenico Church in Cosenza (South Calabria, Italy). *Coatings* **2019**, *9*, 330. [[CrossRef](#)]
26. De los Santos, D.M.; Sanmartin, P.; Rivas, T.; Silva, B.; Mosquera, M.J. A new material with both. In *Proceedings of the International Symposium on Stone Consolidation in Cultural Heritage—research and practice, Lisbon, Portugal, May 6–7 2008*; Delgado, R., Mimoso, J.M., Eds.; Laboratório Nacional de Engenharia Civil: Lisbon, Portugal; pp. 455–462.
27. Pinto, A.P.F.; Rodrigues, J.D. Consolidation of carbonate stones: Influence of treatment procedures on the strengthening action of consolidants. *J. Cult. Herit.* **2012**, *13*, 154–166. [[CrossRef](#)]
28. Teutonico, J.; Charola, A.E.; De Witte, E.; Grassegger, G.; Koestler Robert, J.; Laurenzi Tabasso, M.; Sasse, H.R.; Snethlage, R. Group Report: How Can We Ensure the Responsible and Effective Use of Treatments (Cleaning, Consolidation, Protection)? In *Saving Our Architectural Heritage: The Conservation of Historic Stone Structures*; Dahlem Workshop Report ES20; John Wiley & Sons Ltd.: Hoboken, NJ, USA, 1997.
29. Teutonico, J.M. *A laboratory Manual for Architectural Conservators*; ICCROM: Rome, Italy, 1988; p. 168.
30. Drdácý, M.; Lesák, J.; Niedoba, K.; Valach, J. Peeling tests for assessing the cohesion and consolidation characteristics of mortar and render surfaces. *Mater. Struct.* **2015**, *48*, 1947–1963. [[CrossRef](#)]

31. Scrivano, S.; Gaggero, L.; Gonzalez, A.Y.; Aguilar, J.G. Assessing surface weathering by revision and implementation of the peeling test: In situ sampling and integrated analysis. *J. Cult. Herit.* **2017**, *27*, 88–96. [\[CrossRef\]](#)
32. Becerra, J.; Ortiz, P.; Martín, J.M.; Zaderenko, A.P. Nanolimes doped with quantum dots for stone consolidation assessment. *Constr. Build. Mater.* **2019**, *199*, 581–593. [\[CrossRef\]](#)
33. Wang, R.X.; Yuan, Z.C. The Application of Getting Rc Value from Point Load Test and Rebound Test by Tunnel Surrounding Rock Classification System. *Appl. Mech. Mater.* **2014**, *580*, 1116–1121. [\[CrossRef\]](#)
34. BSI Group. *SR EN 1015-10:2002/A1:2007—Methods for Testing Masonry Mortars—Part 10: Determining the Apparent Density of Hardened Mortar*; British Standards Institution: London, UK, 1999.
35. Japanese Standards Association (JSA). *JIS Z 8729:2004. Color Specification—CIELAB and CIELUV Color Spaces*; Japanese Standards Association (JSA): Tokyo, Japan, 2004.
36. Codarcea, A.; Dimitrescu, R.; Gherasi, N.; Mureşan, M.; Mureşan, G.; Kräutner, H.; Kräutner, F.; Lupu, M.; Marinescu, F.; Savu, H.; et al. *Geological Map of Romania: Deva Sheet, Scale 1:200.000*; Geological Institute of Romania Printing House: Bucharest, Romania, 1967.
37. Danciu, C.; Toderaş, M.; Lorinţ, C.; Florea, A. Characterization and Classification of Andesites of Criscior and Albini from Southern Apuseni Mountains for Capitalization. *Ann. Univ. Petrosani Min. Eng.* **2018**, *19*, 61–69.
38. Balintoni, I. *Geotectonica Terenurilor Metamorfice din România*; Ed. Carpatica: Cluj-Napoca, Romania, 1997; p. 176.
39. Balintoni, I.; Iancu, V. Probleme de metamorfism, litostratigrafie si structura ale cristalinului din masivul Poiana Rusca. *Studii si Cercetari de Geologie, Geofizica si Geografie, seria Geologie, Bucuresti* **1986**, *31*, 51–67.
40. Layani, J.; Mayer, I.; Cuisinier, F. Carbonated hydroxyapatites precipitated in the presence of Ti. *J. Inorg. Biochem.* **2000**, *81*, 57–63. [\[CrossRef\]](#)
41. Rodrigues, J.D.; Grossi, A. Indicators and ratings for the compatibility assessment of conservation actions. *J. Cult. Herit.* **2007**, *8*, 32–43. [\[CrossRef\]](#)
42. BSI. *BS EN 12615:1999: Products and Systems for the Protection and Repair of Concrete Structures-Test Methods-Determination of Slant Shear Strength*; BSI: London, UK, 1999.
43. ISO. 4287:1997—*Geometrical Product Specifications (GPS). Surface Texture. Profile method. Terms, Definitions and Surface Texture Parameters*; International Organization for Standardization: Geneva, Switzerland, 1997.
44. Curray, J.R. The analysis of two-dimensional orientation data. *J. Geol.* **1956**, *64*, 117–131. [\[CrossRef\]](#)
45. Ion, R.-M.; Doncea, S.M.; Ion, M.L.; Rădiţoiu, V.; Amăriutei, V. Surface investigations of old book paper treated with hydroxyapatite nanoparticles. *Appl. Surf. Sci.* **2013**, *285*, 27–32. [\[CrossRef\]](#)
46. Ion, R.-M.; Turcanu-Caruţiu, D.; Fierăscu, R.C.; Fierăscu, I.; Bunghez, I.R.; Ion, M.L.; Teodorescu, S.; Vasilevici, G.; Rădiţoiu, V. Caosite-hydroxyapatite composition as consolidating material for the chalk stone from Basarabi–Murfatlar churches ensemble. *Appl. Surf. Sci.* **2015**, *358*, 612–618. [\[CrossRef\]](#)
47. Ion, R.-M.; Nyokong, T.; Nwahara, N.; Fierascu, I. Wood preservation with gold hydroxyapatite system. *Herit. Sci.* **2018**, *6*, 37. [\[CrossRef\]](#)
48. Ion, R.-M.; Turcanu-Carutiu, D.; Fierascu, R.C.; Fierascual, I. Chalk stone restoration with hydroxyapatite-based nanoparticles. *Sci. Bull. Valahia Univ. Mater. Mech.* **2014**, *9*, 16–19.
49. Wong, W.; Noor, A.-F.M. Synthesis and sintering-wet carbonation of nano-sized carbonated hydroxyapatite. *Proc. Chem.* **2016**, *19*, 98–105.
50. Kovaleva, E.S.; Shabanov, M.P.; Putlyaev, V.I.; Tretyakov, Y.D.; Ivanov, V.K.; Silkin, N.I. Bioresorbable carbonated hydroxyapatite $\text{Ca}_{10-x}\text{Na}_x(\text{PO}_4)_{6-x}(\text{CO}_3)_x(\text{OH})_2$ powders for bioactive materials preparation. *Cent. Eur. J. Chem.* **2009**, *7*, 168–174. [\[CrossRef\]](#)
51. Price, C.; Ross, K. Technical appraisal of stone conservation techniques at Wells Cathedral. In *Conservation of Building and Decorative Stone*; Butterworth/Heinemann: London, UK, 1990.
52. Jerome, P.S.; Weiss, N.R.; Gilbert, A.S.; Scott, J.A. Ethyl silicate as a treatment for marble: Conservation of St. John's Hall, Fordham University. *APT Bull.* **1998**, *29*, 19–26.
53. Weththimuni, M.L.; Licchelli, M.; Malagodi, M.; Rovella, N.; La Russa, M. Consolidation of bio-calcarenite stone by treatment based on diammonium hydrogenphosphate and calcium hydroxide nanoparticles. *Measurement* **2018**, *127*, 396–405. [\[CrossRef\]](#)

54. Kim, H.-W.; Koh, Y.H.; Kong, Y.M.; Kang, K.G.; Kim, H.E. Strontium substituted calcium phosphate biphasic ceramics obtained by a powder precipitation method. *J. Mater. Sci. Mater. Med.* **2004**, *15*, 1129–1134. [[CrossRef](#)]
55. Čadež, V.; Erceg, I.; Selmani, A.; Jurašin, D.D.; Šegota, S.; Lyons, D.M.; Kralj, D.; Sikirić, M.D. Amorphous calcium phosphate formation and aggregation process revealed by light scattering techniques. *Crystals* **2018**, *8*, 254. [[CrossRef](#)]



© 2020 by the authors. Licensee MDPI, Basel, Switzerland. This article is an open access article distributed under the terms and conditions of the Creative Commons Attribution (CC BY) license (<http://creativecommons.org/licenses/by/4.0/>).